Gas-Phase Ethylene Polymerization over Polymer-Supported Metallocene Catalysts

Jia-Min Zhou, Nai-Hong Li, Nai-Yu Bu, David T. Lynch, Sieghard E. Wanke

Department of Chemical and Materials Engineering, University of Alberta, Edmonton, Alberta T6G 2G6, Canada

Received 3 December 2002; accepted 18 February 2003

ABSTRACT: The activities of two (n-BuCp)$_2$ZrCl$_2$ catalysts supported on methylaluminoxane (MAO)-treated polymer particles were evaluated. The supports were spherical polymeric particles, containing macropores and prepared by suspension polymerization of 2-hydroxyethyl methacrylate, divinyl benzene, ethyl styrene, and styrene. Both catalysts had a Zr content of 0.31 mass % and an Al/Zr ratio of 185; the supports for one of the catalysts contained 59 mass % 2-hydroxyethyl methacrylate, whereas the support for the other catalyst had a 2-hydroxyethyl methacrylate content of 10 mass %. Ethylene homo- and ethylene/1-hexene copolymerization activities were determined for gas-phase operation at temperatures of 50 to 90°C and ethylene pressures of ≈1.4 MPa. Polymerization activities were strong functions of temperature and 1-hexene concentration; copolymerization activities of up to 23,200 kg PE/(mol Zr h^{-1}) were obtained for 1-h polymerization runs. The product particle morphology was excellent, mostly spherical particles essentially without fines. Scanning electron microscopy showed that the spherical copolymer particles, for all copolymerization conditions, consisted of well-defined concentric spherical shells. © 2003 Wiley Periodicals, Inc. J Appl Polym Sci 90: 1319–1330, 2003

Key words: metallocene catalysts; supports; gas-phase ethylene polymerization; morphology; copolymerization

INTRODUCTION

A large amount of research dealing with single-site catalysts for olefin polymerization has been published since the discovery by Sinn and Kaminsky[1] that methylaluminoxane (MAO) is a very effective cocatalyst for metallocenes (see, e.g., the recent two volumes edited by Scheirs and Kaminsiky,[2] and various reviews, e.g., Olabisi et al.,[3] Hlatky,[4] and Alt and Köppl[5]). However, the use of single-site catalysts in the commercial production of polyethylenes has been relatively meager in spite of this tremendous amount of research. Currently, only a small fraction of linear low density polyethylene (LLDPE) is produced with metallocene catalysts; according to Foxley,[6] less than 0.5% of all LLDPE produced in Western Europe in 1997 was produced using metallocene catalysts. He estimates that by 2005 over 10% of all LLDPE in Western Europe will be produced by processes using metallocene catalysts. He further predicts that about 70% of the LLDPE made with metallocene catalysts in 2005 will be produced by gas-phase processes; the remainder will be made by solution processes (very low density polyethylenes and elastomers are not included in the mLLDPE amounts). Annual growth rates of over 15% for mLLDPE are expected during the next few years if "the current production, processability and clarity problems will be satisfactorily resolved."[7] The requirements for large amounts of cocatalyst, usually MAO, for homogeneous catalysts,[8,9] reactor fouling for slurry and gas-phase processes,[9–11] and the formation of fines, resulting from fragmentation of the catalyst/polymer particles, in gas-phase processes[4] are some of the operational problems that have to be overcome for large-scale commercialization of metallocene catalysts for the production of LLDPE.

The use of polymeric materials as supports for metallocenes may overcome the operational problems of large MAO requirements, reactor fouling, and fines formation because polymer-supported catalysts frequently produce polyethylene product with good morphology,[12–17] and supported catalysts require smaller amounts of cocatalyst.[4,8] In the current study, we present results for gas-phase copolymerization of ethylene and 1-hexene for two polymer-supported MAO/(n-BuCp)$_2$ZrCl$_2$ catalysts. The supports for these catalysts were spherical, porous polymeric particles prepared in our laboratory by suspension polymerization according to the method described by Li and Mazid[18]; a patent for the use of these polymeric particles as catalyst supports has been granted.[19] The use of polymer supports for olefin polymerization catalysts is not new; various polymers have been used for making supported TiCl$_4$ catalysts,[20–22] and sup-

Correspondence to: S. Wanke (sieg.wanke@ualberta.ca).

Contract grant sponsor: Natural Sciences and Engineering Research Council of Canada (NSERC).

Contract grant sponsor: NOVA Chemicals Corporation.

Journal of Applied Polymer Science, Vol. 90, 1319–1330 (2003)

ported metallocene catalysts.[12–17] The catalysts used in these studies[12–17] had relatively high activities [e.g., 400 to 36,000 kg PE/(mol metallocene h^{-1})]; however, slurry operation was used in all of these studies, with the exception of that by Yu et al.,[17] and only one study by Roscoe et al.[15] reported an activity profile. Yu et al.[17] did not provide details about their gas-phase polymerization studies, and Roscoe et al.[15] provided only one representative activity profile for their study of ethylene/1-hexene slurry copolymerization in hexane. The activation–deactivation behavior of catalyst is very important for commercial use of catalysts, especially for gas-phase applications; very high initial activity can lead to uncontrolled catalyst particle fragmentation, hot spots, and polymer particle agglomeration. Detailed information on activity profiles and effects of operating conditions (e.g., reactor temperature, effect of comonomer amount) for ethylene polymerization during gas-phase operation over polymer-supported metallocenes is not available in the open literature. Such information is presented in the current study for two polymer-supported MAO/(*n*-BuCp)$_2$ZrCl$_2$ catalysts. Detailed information about the morphology of the products is also presented.

EXPERIMENTAL

MATERIALS

Supports

Porous, spherical support particles with different compositions were prepared by suspension polymerization following the method described by Li and Mazid.[18] Briefly, the procedure for the first support consisted of placing 1.0 L of water containing 90 g of acacia, the suspension medium, into a 2-L round-bottom flask equipped with a stirrer and a reflux condenser. The round-bottom flask was placed into a thermostated vessel. The dispersed medium, which contained the monomers, was added to the 2-L flask at 50°C while stirring. The dispersed medium consisted of 26 g of 2-hydroxyethyl methacrylate (HEMA), 18 g of a divinyl benzene (DVB)–ethyl styrene mixture (55 mass % DVB), 30 g of toluene, 2 g of hydrophobic fumed silica (0.1-μm-diameter particles from Cabot Corp.; CAB-SIT-TS-610) and 0.5 g of 2,2′-azobisisobutyronitrile (AIBN) as initiator. The mixture was stirred at 200 rpm as the temperature was increased to 55°C; the temperature was kept at 55°C for 24 h while stirring. The mixture was cooled and the polymer beads, which had formed, were filtered from the suspension by vacuum filtration. The polymer beads were washed several times with water and then dispersed in 300 mL of a 4*M* NaOH aqueous solution containing 50 mL of methanol. The suspension was shaken in a Parr shaker at room temperature for 1 day. The silica in the polymer particles was dissolved by the NaOH solution; the addition of silica to the dispersed phase was used to create macropores in the polymer beads.[18] The polymer beads were filtered from the suspension using a vacuum filter and washed several times with water. The beads were then soaked in methanol for several hours followed by several washings in water and then acetone. The resulting free-flowing solid particles were sieved, and the 200- to 400-μm beads were subsequently used as the support for the catalyst. The second polymeric support was prepared in a similar manner except that the dispersed phase for the suspension polymerization consisted of 4.5 g of HEMA, 20.25 g of the DVB–ethyl styrene mixture, 20.25 g of styrene, 30 g of toluene, 0.5 g of AIBN, and 2 g of fumed silica. The acacia, HEMA, styrene, DVB–ethyl styrene mixture, toluene, and AIBN were obtained from Aldrich (Milwaukee, WI). The HEMA, styrene, and DVB–ethyl styrene mixture were passed through an inhibitor-removal column (Aldrich) before use; the other materials were used as received.

The first support, which contained a nominal 59 mass % HEMA, will be referred to as HEMA59, and the second support, which contained a nominal 10 mass % HEMA, will be referred to as HEMA10. Micrographs of HEMA10 support particles and the HEMA10-supported catalyst (CAT-B, described below) are shown in Figure 1. As shown in Figure 1(a) and (c), most of the support and catalyst particles are spherical. The higher magnification micrographs in Figure 1(b) and (d) show the macroporous structure of the support and the catalyst. The catalyst appears to have fewer and somewhat smaller macropores; this is probably the result of the partial filling of the pores by MAO. The structures of the HEMA59 and the catalyst made with the HEMA59 (CAT-A) were very similar to those shown in Figure 1.

Catalysts

Two catalysts, CAT-A with the HEMA59 support and CAT-B with the HEMA10 support, were prepared by impregnation of the supports with methylaluminoxane (MAO) and (*n*-BuCp)$_2$ZrCl$_2$. The impregnation procedure consisted of putting 2 g of support into a 250-mL flask containing 20 mL of anhydrous toluene under nitrogen. The flask was evacuated for 2 h at 60°C before the addition of nitrogen and 20 mL toluene. The slurry was shaken at room temperature, using a Thermolyne Maxi-Mix III shaker (Fisher Scientific), while 13.3 mL of a 10 mass % MAO in toluene solution was added slowly to the slurry. Gas evolution was observed during this addition. The slurry was stirred for 12 h at room temperature. Subsequently, a toluene solution containing 44.3 mg of (*n*-BuCp)$_2$ZrCl$_2$ was injected into the slurry using a Hamilton gas-tight syringe. The reaction was continued for 4 h at room temperature, followed by evaporation to dryness un-

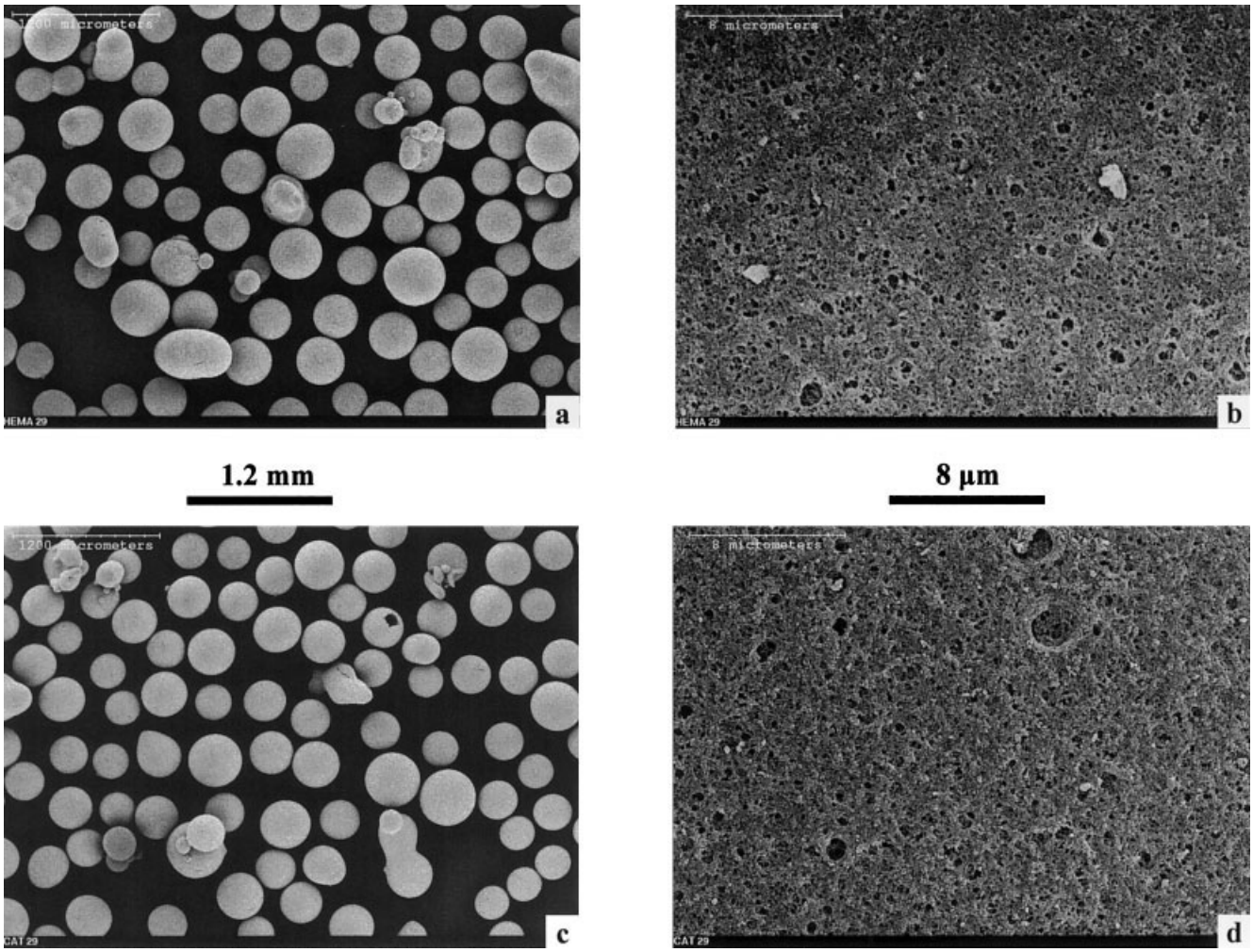

Figure 1 Scanning electron micrographs. (a) and (b): Support HEMA10; (c) and (d): CAT-B.

der vacuum until the catalyst become a free-flowing solid. The contents of Zr and Al in the catalyst were estimated as [Al] = 6.3 mmol per g of catalyst, [Zr] = 0.034 mmol/g of catalyst; this corresponds to an Al : Zr ratio of about 185. The catalysts were stored in a glove box until used. [The MAO was purchased from Aldrich and the $(n\text{-BuCp})_2ZrCl_2$ was donated by NOVA Chemicals; both were used as received.]

Polymerization procedure

A 1-L stainless steel reactor, immersed in a circulating oil bath for temperature control, was used for the polymerizations. The solids in the gas-phase reactor were kept in suspension by an AE Magne-Drive stirrer (Autoclave Engineers). Six thermocouples were located at various radial and axial positions inside the reactor (see Fig. 2 for schematic diagram). Measurement of temperature as a function of position, as well as time, is important for gas-phase polymerization because significant bulk temperature gradients can exist during gas-phase polymerization with high-activity catalysts, even at high stirring rates. The procedure for gas-phase polymerization runs consisted of the following steps:

1. Sodium chloride particles (80 g with a diameter ~ 0.5 mm) were placed into the clean reactor (the NaCl improved heat transfer and improved the suspension of the catalyst/polymer particles).
2. The reactor was attached to the feed system and pressure tested at room temperature with nitrogen at 2 MPa.
3. If leak-free, the reactor was then surrounded by a circulating silicone oil bath at 90°C and evacuated overnight.
4. The next morning, the reactor was cooled to the desired temperature.
5. The reactor was filled to 0.2 MPa with nitrogen and then evacuated for 10 min.
6. The reactor was then charged with ethylene to 0.14 MPa; for copolymerization runs, the desired amount of 1-hexene was added to the

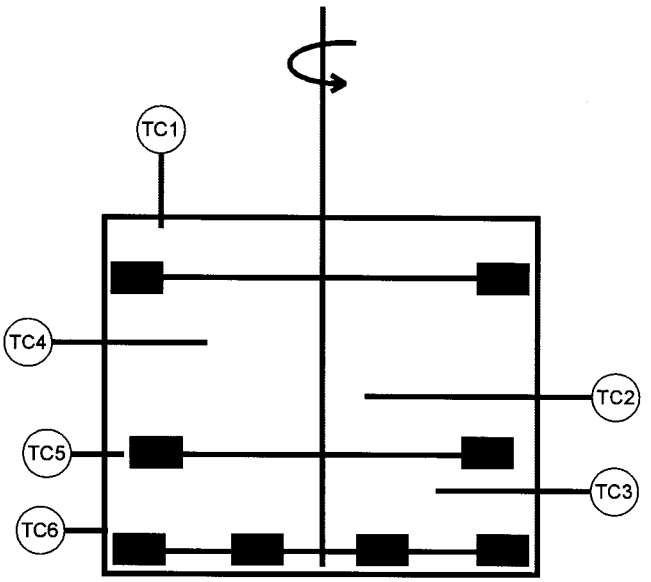

Figure 2 Schematic diagram of reactor showing location of thermocouples TC1 to TC6.

reactor with an ISCO Model 500D syringe pump.

7. The desired amount (0.10 or 0.15 mL) of neat triisobutylaluminum (TIBA) was injected into the reactor with a Hamilton gas-tight syringe followed by addition of ethylene to a total pressure of 0.7 MPa.
8. The reactor contents were stirred for 30 min (scavenging of impurities by the TIBA).
9. The desired amount of dry catalyst was injected into the reactor by flowing ethylene using a high-pressure injector that had been charged with the catalyst in the glove box; ethylene was added until the total pressure in the reactor was about 1.4 MPa.
10. Ethylene was added continuously throughout each run to maintain the reactor at about 1.4 MPa.
11. At the end of the run the gases were vented from the reactor, the reactor was flushed with nitrogen, and air was admitted into the reactor.

Polymer-grade ethylene from Matheson was purified by passage through three fixed-bed purifiers from Altech containing BASF R3-11, Ascarite, and 3-Å molecular sieves before entering the reactor. The polymer-grade 1-hexene was donated by NOVA Chemicals and was used without additional purification. The feed rate of ethylene to the reactor, the reactor pressure, and the output from the six thermocouples were recorded by the data acquisition system at 10-s intervals. The instantaneous polymerization rate was calculated from the instantaneous feed rate of ethylene to the reactor. Additional details of the reactor system and general operating procedures were described previously.[23]

Characterization of polyethylene

The molar masses of the products were measured by size-exclusion chromatography (SEC) using an Alliance 2000 GPCV equipped with a series of three Waters HT6E columns (Waters Chromatography Division/Millipore, Milford, MA). The detectors and the columns were maintained at 145°C; the flow rate of the solvent, HPLC-grade 1,2,4-trichlorobenzene (from Fisher Scientific, Pittsburgh, PA), was 1.0 cm^3/min. About 0.25 g/L of the antioxidant 2,6-*tert*-butyl-4-methylphenol (Sigma-Aldrich) was added to the 1,2,4-trichlorobenzene. Amounts of polyethylene in 1,2,4-trichlorobenzene samples at concentrations of 0.5 to 0.7 mg/mL were injected into the SEC for molar mass determinations. Polystyrene standards (from TSK Standards), linear paraffins (C_{20}, C_{40}, and C_{60}) and polyethylene reference materials 1482, 1483, and 1484 from NIST were used as calibration standards.

A Hitachi S-2700 scanning electron microscope (SEM) was used to examine the morphology of supports, catalysts, and polymer particles. Polymer particles were cut at room temperature with a scalpel or fractured, after having been cooled in liquid nitrogen, to examine the interior structure of particles. Samples were carbon and gold coated before examination in the SEM. The images were recorded in digital format. The bulk density of the products was measured according to the ASTM D 1895-96 procedure.

RESULTS AND DISCUSSION

Kinetic behavior

The conditions at which the gas-phase polymerization activities of the HEMA-supported catalyst were measured are listed in Table I. The type of data gathered for each run is illustrated in Figure 3 for runs with CAT-B. The three panels in Figure 3 show the temperature, ethylene polymerization activity, and pressure as a function of time for the runs with CAT-B with the lowest activity (Run B-3) and the run with the highest activity (Run B-9). The top panel shows the pressures before and after injection of the catalyst; zero time corresponds to the injection of the catalyst. The rates of ethylene addition, which are approximately equal to the rate of ethylene polymerization, are shown in the center panel. The high "rates" at time = 0 are attributed to the ethylene flow required to increase the pressure in the reactor; blank runs have shown that the reactor filling is complete in less than 2 min. The bottom panel shows the temperature as measured by TC5 (see Fig. 2). The small spike in temperature at time = 0 is attributed to the essentially adiabatic com-

TABLE I
Conditions and Activities for Ethylene Gas-Phase Polymerization over HEMA-Supported Metallocene Catalysts

Run no.[a]	Mass of catalyst (mg)	Amount of TIBA (mL)	C_2H_4 pressure (MPa)	Amount 1-C_6H_{12}[b] (mL)	T[c] (°C)	Run time (h)	PE yield (g)	Activity[d] [kg PE/(g catalyst h^{-1})]	
								R_{max}	R_{avg}
A-1	124	0.15	1.4	0	90	2.30	17.4	0.18	0.06
A-2	60	0.10	1.4	1.4	90	1.01	30.4	1.12	0.50
A-3	56	0.10	1.4	1.6	90	1.02	35.8	1.17	0.63
A-4	60	0.10	1.4	1.6	80	1.06	50.0	1.84	0.79
A-5	59	0.10	1.5	1.6	70	1.37	38.2	0.68	0.47
A-6	59	0.10	1.4	1.7	50	2.17	9.3	0.08	0.07
B-1	88	0.10	1.4	0	80	0.88	<1	<0.01	<0.01
B-2	144	0.10	1.4	0	80	1.08	<1	<0.01	<0.01
B-3	152	0.15	1.4	0	80	1.01	<1	<0.01	<0.01
B-4	151	0.10	1.4	0	50	1.15	2.8	0.06	0.02
B-5	63	0.10	1.3	1.6	90	1.01	7.9	0.18	0.12
B-6	88	0.10	1.4	1.7	80	1.00	20.5	0.34	0.23
B-7	70	0.10	1.4	1.6	70	1.05	5.4	0.09	0.07
B-8	94	0.10	1.3	2.7	80	0.99	65.9	1.45	0.71
B-9	102	0.15	1.2	2.7	80	1.01	60.7	1.53	0.59

[a] Prefix A- is for runs with CAT-A and prefix B- is for runs with CAT-B.
[b] Amount of liquid 1-hexene added to reactor at beginning of run.
[c] Initial temperature (see Fig. 3 to 5 for temperature profiles during runs).
[d] Maximum rates were calculated from the ethylene feed rates and average rates were calculated from the amount of PE made.

pression during filling, and this small temperature spike is a very useful marker for accurate determination of the time of catalyst injection. The temperature profiles in the bottom panel of Figure 3 show that the bulk gas-phase temperature can increase significantly from the initial temperature. Thermocouples TC3 and TC5 indicated the highest temperatures for all the runs because most of the polymerization occurred in the region in which thermocouples TC3 and TC5 are located. The temperature variations, with time as indicated by the various thermocouples, are shown in Figure 4 for Run B-9. These are the maximum temperature variations observed in this study for both CAT-A and CAT-B. Most studies do not provide details about the method used to measure the reaction temperature. For slurry polymerizations, temperatures usually do not vary much either with position or with reaction time. This is not the case for gas-phase polymerizations, and the above results clearly indicated the need to monitor the interior temperatures in the reactor during gas-phase polymerization. Measure-

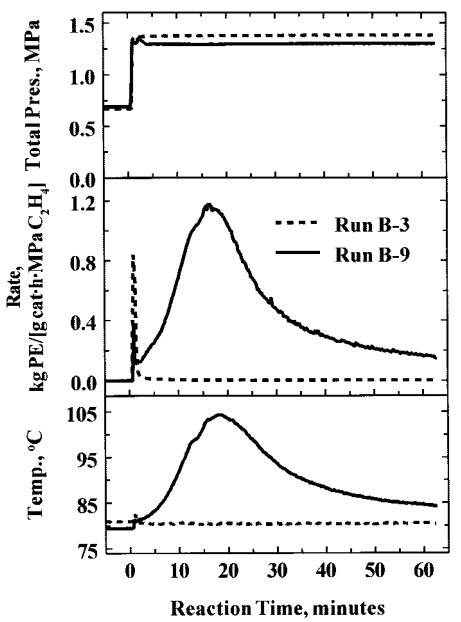

Figure 3 Temperature, activity, and pressure profiles for homopolymerization (Run B-3) and copolymerization (Run B-9).

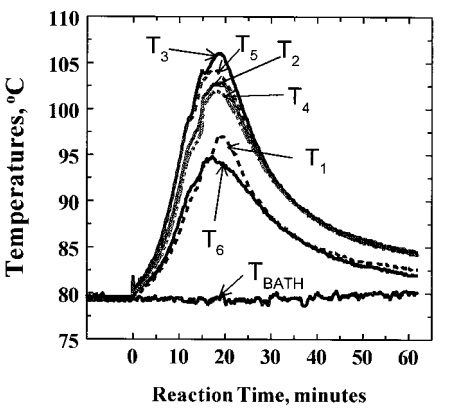

Figure 4 Temperature at various locations in the reactor as a function of time for Run B-9.

ment of the cooling fluid temperature or the reactor wall temperature is insufficient for establishing the reaction temperature.

Comparison of homopolymerization and ethylene/1-hexene copolymerization

The ethylene homopolymerization activities were very low for both of the catalysts (see results for Runs A-1 and B-1 to B-3 in Table I and activity profile in Fig. 3 for Run B-3). The very low homopolymerization activity of CAT-B was unexpected. For this reason two repeat runs (Runs B-2 and B-3) were done to confirm the low activity observed for Run B-1 (Runs B-5 to B-8 were done after Run B-1 and before B-2, and Run B-9 was done after Run B-2 and before B-3). It is important to mention the sequence of the runs because we have observed anomalously low activities for a number of sequential runs as a result of undetected reactor contamination. This was not the case for the low homopolymerization observed for both CAT-A and CAT-B, given that high activities were observed for the copolymerization runs done between the homopolymerization runs.

Activities for ethylene/1-hexene copolymerization were much higher than the homopolymerization activities (cf. activities in Table I for Runs A-1 with A-3, and Runs B-1 to B-3 with Run B-6 and B-8). The low homopolymerization activities were not attributed to the differences in the temperature profiles for homo- and copolymerization because the homopolymerization activity for catalyst CAT-B was significantly higher at 50 than at 80°C (cf. Runs B-4 with Runs B-1 to B-3). Homo- and copolymerization profiles for CAT-A and CAT-B are compared in Figure 5 (activities are plotted on a logarithmic scale to clearly show activity trends). The initial activity of CAT-A for homopolymerization at 90°C is higher than the initial copolymerization activity. For CAT-B, the initial homopolymerization activity at 50°C is higher than the initial copolymerization activity at 70°C. This suggests that rapid deactivation occurs under homopolymerization conditions. The presence of 1-hexene resulted in lower rates of activation as well as lower rates of deactivation (see activity profiles in Fig. 5). This suggests that the activation and deactivation characteristics were mainly the result of chemical changes of the active sites and not solely the result of physical processes as proposed by Roscoe et al.[15] Our results suggest that 1-hexene interacts with the catalytic sites in the HEMA-supported MAO/(*n*-BuCp)$_2$ZrCl$_2$ catalysts resulting in a suppression of the initial rates; the TIBA, added as a scavenger, may also have interacted with the catalytic sites. Activity increases as these dormant sites become activated by interaction with ethylene. The activation and deactivation during copolymerization are extremely temperature sensitive as shown below.

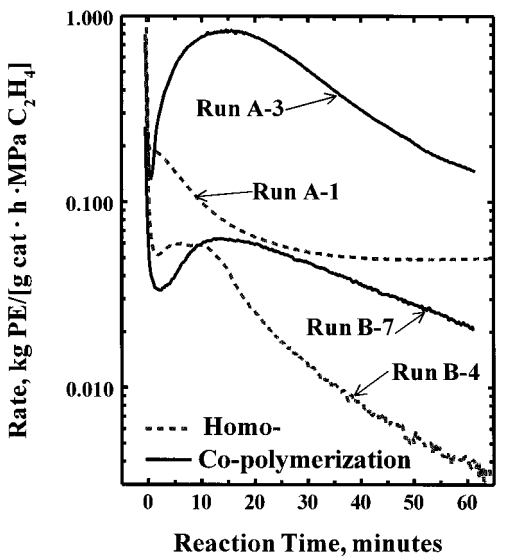

Figure 5 Comparison of homo- and copolymerization runs for CAT-A and CAT-B.

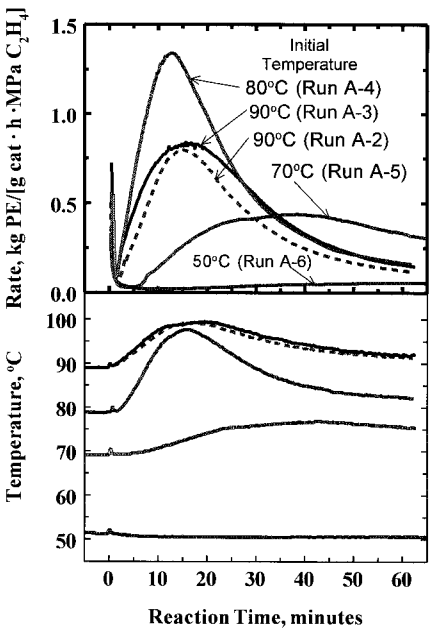

Figure 6 Activity and temperature profiles for copolymerization for CAT-A as a function of initial reactor temperature (Runs A-2 to A-6).

Effect of temperature on copolymerization activity

Activity and temperature profiles (thermocouple TC5) for various initial reactor temperatures are shown in Figures 6 and 7 for CAT-A and CAT-B. The activities in Figures 6 and 7 have been normalized with respect to catalyst mass and ethylene pressure. Two runs were done with CAT-A at an initial temperature of 90°C

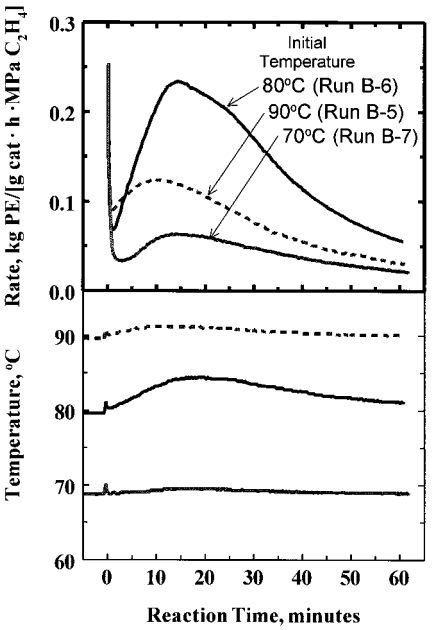

Figure 7 Activity and temperature profiles for copolymerization for CAT-B as a function of initial reactor temperature (Runs B-5 to B-7).

(Runs A-2 and A-3); Run A-2 had slightly lower 1-hexene and ethylene concentrations; nevertheless, the reproducibility of the activity and temperature profiles is reasonably good. Average and maximum activities are shown in Figure 8. These results show that activity profiles as well as overall activities were strong functions of the initial reactor temperature. Average and maximum activities increased as the initial reactor temperature was increased from 50 to 80°C and then decreased as the initial reactor temperature was increased to 90°C. This behavior was observed for both CAT-A and CAT-B. It can be argued that poor control of the bulk gas-phase temperature for runs with CAT-A was largely responsible for the activation–deactivation behavior of CAT-A; the bulk gas-phase temperatures increased by as much as 15°C (see Fig. 6). However, similar behavior was observed for CAT-B and for these runs no large increases in bulk gas-phase temperature were observed (see Fig. 7). It is more likely that the activation–deactivation is the result of large temperature increases inside the growing polymer/catalyst particles during the initial stages of the polymerization. According to the results in Figures 6 and 7, deactivation rates increase more rapidly than activation rates with increasing temperature. The activation rates for copolymerization over CAT-A at 50°C (Run A-6) were very slow and the deactivation rates were even slower because the activity increased throughout the 2.2 h. The different temperature dependencies of the activation and deactivation processes resulted in maximum activities for these HEMA-supported catalysts at bulk gas-phase temperatures of 80 to 90°C. The shapes of the activity profiles for CAT-A and CAT-B are similar; however, the activity profiles for CAT-B are flatter. The profiles for CAT-B are flatter than those of CAT-A because the temperature increases for CAT-B were considerably less than those for CAT-A; the higher temperature for CAT-A resulted in more rapid deactivation. Chemical changes in the active sites were the probable cause of the deactivation. It is unlikely that changes in the permeability of the monomers through the produced LLDPE, as proposed by Roscoe et al.,[15] was the cause for the decrease in activity.

Comparison of CAT-A with CAT-B and effect of 1-hexene concentration

The activity of CAT-B for homopolymerization was much lower than that of CAT-A (see Table I and Fig. 5). The copolymerization activity of CAT-B was also much lower than that of CAT-A at similar 1-hexene concentrations. The average and maximum activities of CAT-A and CAT-B as a function of initial reactor temperature, with an initial charge of about 1.6 mL of 1-hexene and normalized with respect to ethylene pressure, are shown in Figure 8. The maximum specific activity for both catalysts occurred at an initial reactor temperature of 80°C. This observation, along with the similarity of the shapes of the activity profiles for CAT-A and CAT-B, suggests that the active sites are similar for both catalysts; however, the number, accessibility, and specific activity of the active sites of the two catalysts were different even though the total $(n\text{-BuCp})_2ZrCl_2$ and MAO loading for the two catalysts were the same. Additional investigations are needed to determine whether the composition of the supports (HEMA59, the support for CAT-A, had a higher concentration of hydroxyl and ester groups

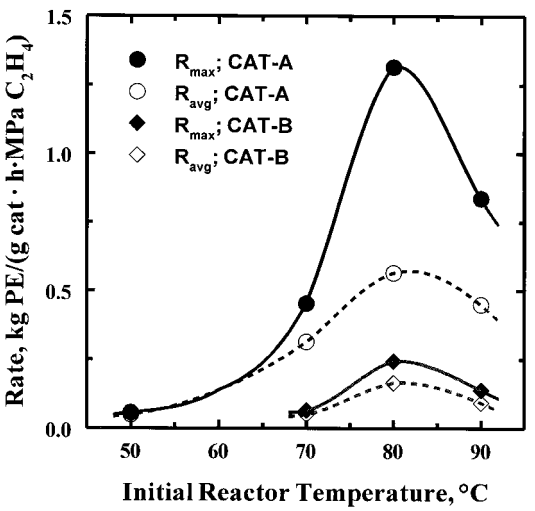

Figure 8 Maximum and average rates for CAT-A and CAT-B as a function of initial reactor temperature.

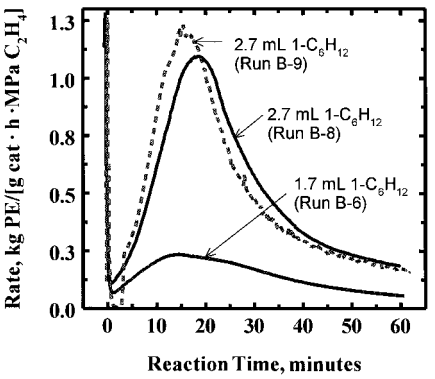

Figure 9 Effect of 1-hexene concentration on ethylene polymerization activity profiles for CAT-B.

than that of HEMA10) or the structure of the supports was responsible for the difference in activity. SEM results indicated the macroporous structure of HEMA59 and HEMA10 were similar, but the meso and microporous structures may have been different.

Two runs (Runs B-8 and B-9) were done with CAT-B at higher initial 1-hexene concentrations (2.7 mL 1-hexene for Runs B-8 and B-9, compared to 1.7 mL for Run B-6). This increase in 1-hexene resulted in a threefold increase in average activity for the 1-h runs with an initial reactor temperature of 80°C. Activity profiles for these runs are shown in Figure 9. The activity profiles for the two runs with 2.7 mL 1-hexene (Runs B-8 and B-9) are very similar even though the amount of TIBA and the ethylene pressures were somewhat different for the two runs. This indicates that the 1-hexene concentration was the main cause for the increase in activity.

The reason for this sensitivity to 1-hexene is not known, although it is similar to the poorly understood comonomer effect commonly observed for $MgCl_2$-supported $TiCl_4$ catalysts.[25,26] Galland et al.[27] observed that catalytic activity was sensitive to comonomer concentration during the copolymerization of ethylene and 1-hexene in slurry polymerization using MAO-activated homogeneous and silica-supported $(n\text{-BuCp})_2ZrCl_2$ catalysts; copolymerization activities were higher than homopolymerization activities. Galland et al.[27] attributed the increased activity in the presence of 1-hexene to higher solubility of the copolymer in the toluene; it was postulated that this results in higher diffusion rates. The solvation of polymer cannot be used as an explanation for increases in polymerization activity in the current gas-phase polymerization. It is possible that diffusion resistances are lower in the copolymer compared to those in the homopolymer, but it is unlikely that the lower crystallinity of the copolymer can cause decreases in diffusion resistances that result in an over fourfold increase in the maximum polymerization rate (cf. maximum rates in Table I for Runs B-6 with B-8 and B-9). More detailed studies on the effect of 1-hexene concentration on polymerization rates and product properties are required to provide insight into the causes of the 1-hexene effect on rates.

Comparison of CAT-A and CAT-B activities with values in the literature

As mentioned above, there are very few studies in the open literature that deal with gas-phase polymerization of supported metallocene catalysts. The number of studies that report activities normalized with respect to metallocene concentration is even fewer. Activity results from a few studies, including a gas-phase study with a silica-supported metallocene catalyst, are summarized in Table II. These results show that the average activity for both CAT-A and CAT-B are higher than any of those reported for gas-phase poly-

TABLE II
Comparison of Activities of Supported Metallocene Catalysts in Slurry and Gas-Phase Ethylene Polymerizations

Support	Catalyst	Cocatalyst Type	Cocatalyst Al/Metal	T (°C)	Phase	C_2H_4 pressure (MPa)	Comonomer	Activity [kg PE/(mol metallocene h^{-1})]	Ref.
HEMA59	$(n\text{-BuCp})_2ZrCl_2$	MAO	185	80	Gas	1.4	1-C_6H_{12}	23,200	This study
HEMA10	$(n\text{-BuCp})_2ZrCl_2$	MAO	185	80	Gas	1.2	1-C_6H_{12}	20,900	This study
Silica	$Me_2Si[Ind]_2ZrCl_2$	MAO	383	80	Gas	0.5	None	3,500	28
Polymer[a]	Cp_2ZrCl_2	MAO	300	60	Gas	—[b]	1-C_4H_8	1,100	17
Polymer[a]	Cp_2ZrCl_2	MAO	600	90	Gas	—[b]	None	11,500	17
Polymer[a]	Cp_2ZrCl_2	MAO	500	80	Slurry	1.0	None	36,200	17
PS[c]	Cp_2ZrCl_2[d]	MAO	2000	70	Slurry	4.0	None	6,660	16
PS/DVB[c]	Metallocene[e]	Borate	—	40	Slurry	0.5	1-C_6H_{12}	3,200	15

[a] No details on polymer provided except that it is commercially available.
[b] Ethylene pressure not given.
[c] PS, polystyrene; DVB, divinylbenzene.
[d] Synthesized *in situ*.
[e] Metallocene is not specified in table of activities; bis(tetramethylcyclopentadienyl) dimethylhafnium is given as an example.

TABLE III
Properties of Polyethylene Product as Function of Polymerization Conditions

Run no.	T (°C)	M_w ($\times 10^{-3}$)	M_w/M_n	Bulk density (g/cm^3)	Product particle size distribution mass % in size ranges		
					<0.5 mm	0.5 to 2 mm	>2 mm
A-1	90	102	2.9	0.37	7.5	12.1	80.4
A-2	90	96	2.2	0.36	0.5	6.9	92.6
A-3	90	95	2.5	0.25	0.2	4.2	95.6
A-4	80	95	2.3	0.29	0.9	2.8	96.3
A-5	70	98	2.5	0.38	0.6	5.5	93.9
A-6	50	94	2.9	0.35	0.6	21.4	78.0
B-2[a]	80	Not measured		0.38	40.5	59.5	0.0
B-3[a]	80	106	3.3	0.31	48.8	51.2	0.0
B-4[b]	50	187	2.5	0.38	67.6	26.7	5.7
B-5	90	85	3.7	0.39	tr[c]	28.0	72.0
B-6	80	88	2.6	0.37	tr	1.5	98.4
B-7	70	102	2.8	0.39	tr	38.8	61.2
B-8	80	100	2.3	0.23	1.7	3.0	95.3
B-9	80	95	2.7	0.28	2.0	4.9	93.1

[a] Almost all particles were spherical; small size due to low yield.
[b] Most particles < 0.5 mm were irregularly shaped; particles 0.5 to 2 mm were mostly spherical; particles > 2 mm were irregularly shaped aggregates.
[c] tr, trace amounts (< 0.1 mass %).

merization even though the Al/Zr ratio used in the current study was considerably lower than those used in other studies reported in Table II. The activity for slurry polymerization in the recent study by Yu et al.[17] was higher than that for CAT-A and CAT-B, but a relatively high Al/Zr ratio of 500 was used to obtain this rate. Good product morphology was reported in all the studies with polymer-supported catalysts listed in Table II, but Roscoe et al.[15] mentioned that increasing the reaction temperature from 40 to 60°C resulted in a large increase in rate accompanied by a "considerable exotherm" and small polymer product particles with poor morphology of variable and ill-defined shapes. As discussed in the following section, all the copolymerizations reported in this study resulted in products with good morphology and spherical shape even at average rates severalfold higher than those obtained by Roscoe et al.[15]

Product properties

Molar masses, bulk densities, and size distribution information for the polymer products are tabulated in Table III. The molar masses of product made with CAT-A were essentially independent of polymerization conditions; all the copolymers had weight-average molar masses (M_w) of 96,000 (±2000) and the homopolymer had an M_w of 102,000. The polydispersities of these samples were all in the 2.2 to 2.9 range, indicating that CAT-A was essentially a single-site catalyst. The variation of M_w for products made with CAT-B was larger, and the only apparent trend in the M_w values for the copolymers was a decrease in M_w with increasing reaction temperature. The homopolymer made at 80°C had an M_w value higher than those of the copolymers and the homopolymer made at 50°C had a significantly higher M_w. The polydispersities of the products made with CAT-B ranged from 2.3 to 3.7; this indicates that the catalytic sites in CAT-B were more heterogeneous than those in CAT-A. The same preparation procedure was used for CAT-A and CAT-B; hence the differences in the nature of the active sites were probably attributable to the difference in the nature of the supports. However, studies with polymeric supports of different composition and structure are required to substantiate this speculation.

The bulk (apparent) densities ranged from 0.23 to 0.39 g/cm^3; a procedure similar to the procedure described in Test Method A, ASTM D 1895-96 was used to measure the bulk densities, but smaller samples than required by the method were used because the total amount of product made was less than 100 g for all the runs. The bulk densities are a function of the polymerization rate; this relationship is shown in Figure 10. The bulk densities were about 0.35 to 0.39 when the maximum polymerization rate was less than about 1.1 kg PE/(g catalyst h^{-1}); at higher rates the bulk density decreased to the 0.23 to 0.29 g/cm^3 range. This was true for products made with both CAT-A and CAT-B. The reason for this drop in density must be the result of the internal morphology (porosity) of the polymer particles because most of the particles were spherical in shape.

The products from all the runs, with the exception of the product from Run B-4, consisted mostly of spherical particles; the average size of the particles increased with increasing total yield. The products were essentially free from fines, and the very small

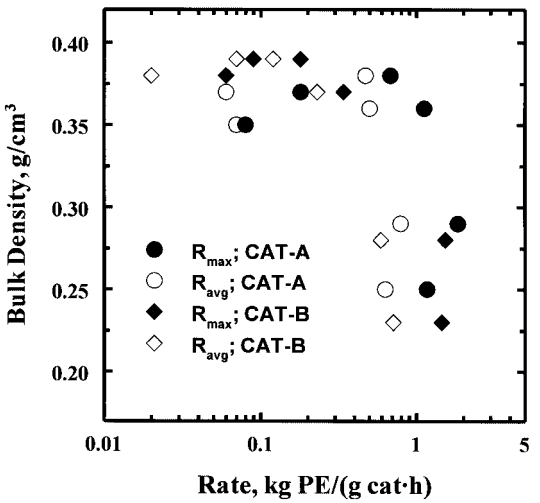

Figure 10 Relationship between polymerization rate and bulk density.

amounts of fines were probably formed by the grinding action of the NaCl. An indication of the distribution of particle sizes is given in the last three columns of Table III. The reason for the irregularly shaped particles from Run B-4 (homopolymerization at 50°C) is not known. It appears that many of the catalyst particles disintegrated and this can only be attributed to a high reaction rate very early in the run, given that subsequent polymerization rates were low compared to runs in which particle disintegration did not occur.

Product particle morphology

Scanning electron microscopy was used to examine the external and internal structure of the polyethylene particles; representative micrographs are shown in Figure 11. The micrographs in the left-hand column of Figure 11 illustrate the typical exterior of the spherical polyethylene particles. The particles were essentially spherical, but the exterior surface of the particles was rough. The irregular exterior appearance of these particles suggests that the particles are an agglomeration of smaller particles; however, the cross section of the particles shown in the micrographs in the middle column of Figure 11 show that this is not true.

The interior structure of the homopolymer [Fig. 11(b)] consists of large aggregates (chunks) separated by micron-sized cracks; this structure is similar to that observed by Kittilsen et al.,[29] and McKenna and Soares[30] postulated that such structures result in reduced mass transfer resistances. The interior structure of all the copolymers was markedly different from that of the homopolymers; representative micrographs of cross sections of copolymers particles from Runs A-3, A-4, B-6, and B-8 are shown in the center column of Figure 11. It should be pointed out that all copolymer particles examined by SEM from all the copolymerization runs listed in Table I had the concentric spherical-shell structure shown in Figure 11. This structure is similar to that observed for polypropylene made by the Spheripol process.[31] Galli and Haylock[31] stated that diffusion-controlled polymer particle growth results in a layered internal structure for the polymer particles, whereas a random internal structure results for reaction-controlled polymerization. A mathematical model for the formation of such structures has recently been presented by Kittilsen et al.[29]; the model is based on spatial variations in particle growth rate inside the polymer particles. This variation in growth rates is attributed to mass transfer limitations, which cause internal tensions in the particles causing internal rupturing of the particles. The predictions of this model are in qualitative agreement with the observed morphology of the copolymer particles produced in the current study, but the sensitivity to particle size and polymerization rate predicted by the model is not in quantitative agreement with our observations because all the copolymer particles examined in this study, regardless of rate or size, had the concentric shell structure and none had a hollow center. However, the rates and the particles used in the model and in those obtained in our experiments were not the same. The concentric shell structure was observed in this study at copolymerization rates lower than the homopolymerization rates for Run A-1, which did not result in concentric shell formation; this suggests that factors other than mass transfer also play a role in the morphology development of polymer particles.

Micrographs at higher magnifications are shown in the final column of Figure 11. Figure 11(c), for the homopolymer, shows a fibrous structure with many of the fibers broken; this indicates inhomogeneous expansion of the growing polymer particles. The broken, cold-drawn fibers were a common interior feature of homopolymer particles. Such fibers were largely absent in the copolymers. To ensure that the lack of detection of fibers in copolymer particles was not the result smearing of the surface during cutting with a scalpel at room temperature, several samples were fractured after having been cooled in liquid nitrogen. The specimens used for Figure 11(i,l) were made by fracturing in liquid nitrogen; these samples also did not show any of the fibrous structure. The fine structures in Figure 11(i) are not fibers but fracture surfaces resulting from fracture at low temperatures. Homopolymer particles from Run A-1, fractured in liquid nitrogen, had a fibrous structure similar to that shown in Figure 11(c). The absence of fibers in the copolymers suggests that the presence of 1-hexene allows internal rupturing of growing polymer particles without cold drawing and ruptur-

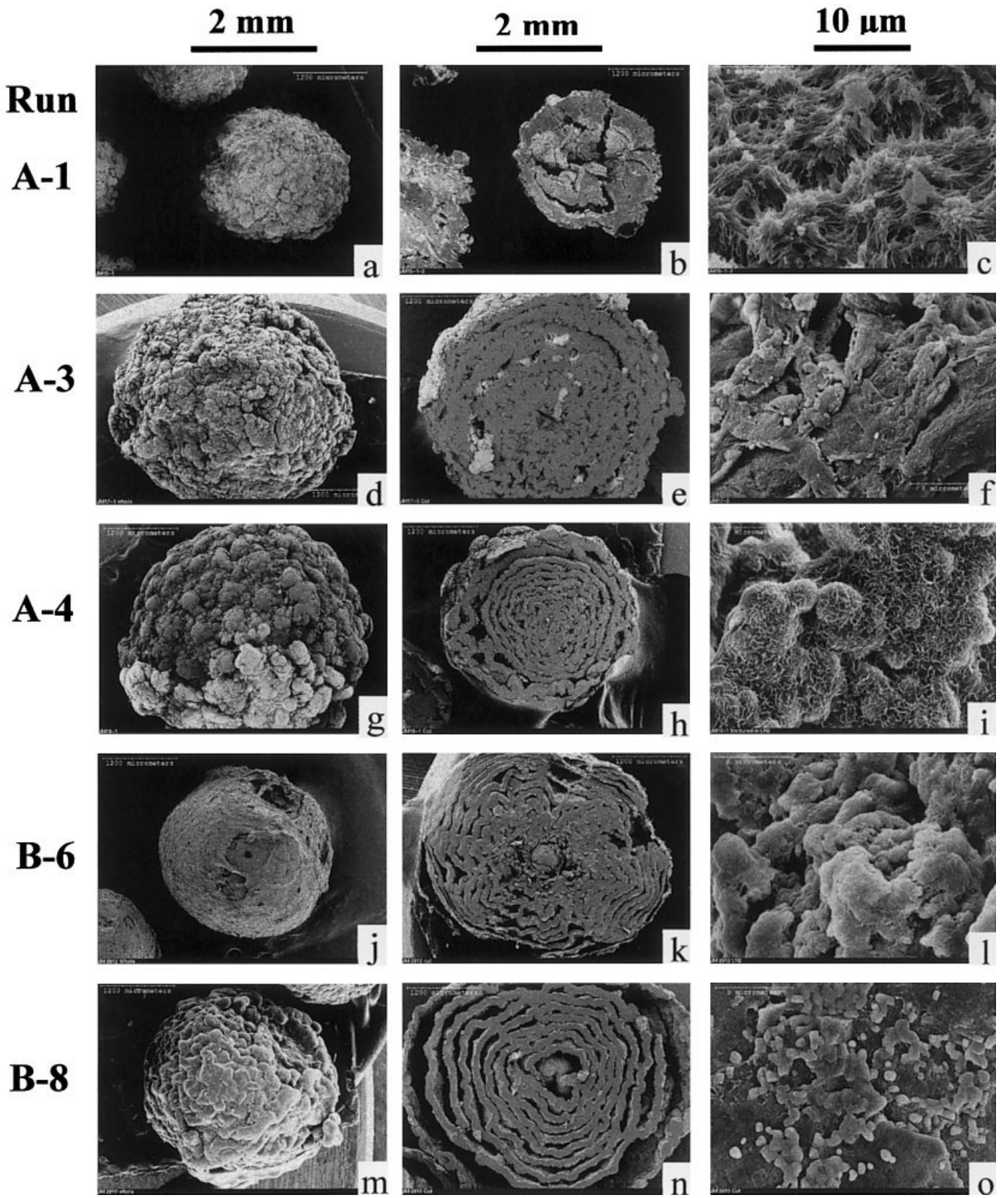

Figure 11 Scanning electron micrographs of product particles.

ing of fibers. Localized dissolution of polymer molecules by sorbed 1-hexene could be responsible for the absence of fiber formation during copolymerization. Mulder[32] observed recrystallization during the sorption of 1-butene and 1-hexene by polyethylenes. Additional polymerization studies over a wide range of polymerization rates, comonomer concentrations, and particle sizes, coupled with SEM char-

acterization, are required to quantify the factors responsible for the internal morphology of the copolymer particles.

CONCLUSIONS

Polymer-supported metallocene catalysts, activated with MAO (Al/Zr = 185), which are very active for 1-hexene/ethylene copolymerization in gas-phase operation, were synthesized. These catalysts produce copolymer particles with excellent morphology without the need for prepolymerization. The catalysts were prepared by a very simple impregnation method, and only one concentration of $(n\text{-BuCp})_2ZrCl_2$ and a fixed MAO/metallocene ratio was used; optimization of $(n\text{-BuCp})_2ZrCl_2$ content and Zr/MAO ratio should result in catalysts with higher activities. The variation of polymerization rate and product molar mass dispersity with changes in the polymer support (HEMA59 and HEMA10) leads to the conclusion that polymeric catalyst supports are not inert participants in the catalysts as is sometimes assumed.[15,16]

The polymerization activity was very sensitive to temperature, with highest activities in the 80 to 90°C range. For CAT-B, the polymerization rates were a strong function of 1-hexene concentration. The dependency of the rate on temperature and 1-hexene concentration along with the dependency of the shape of the activity profiles on temperature lead to the conclusion that chemical changes of the catalytic sites, rather than physical processes such as particle swelling and changes in permeability of polymer particles to monomers, were responsible for the activation–deactivation characteristics of the catalysts. Copolymer particles consisted of concentric spherical shells; this shell structure occurred for both low and high polymerization rates; hence it can be concluded that factors other than, or in addition to, mass transfer are involved in the development of the internal morphology of the growing polymer particles.

The authors acknowledge the support of this work by the Natural Sciences and Engineering Research Council of Canada (NSERC) and NOVA Chemicals Corp.

References

1. Sinn, H.; Kaminsky, W. Adv Organomet Chem 1980, 18, 99.
2. J.; Scheirs, W. Kaminsky, Eds. Metallocene-based Polyolefins: Preparation, Properties, and Technology; Wiley: West Sussex, UK, 2000.
3. Olabisi, O.; Atiqullah, M.; Kaminski, W. J Macromol Sci Rev Macromol Chem Phys 1997, C37, 519.
4. Hlatky, G. Chem Rev 2000, 100, 134.
5. Alt, H. G.; Köppl, A. Chem Rev 2000, 100, 1205.
6. Foxley, D. Chem Ind 1998, 9, 305.
7. Chemical Industries Newsletter, SRI Consulting, 2000, 3, 1.
8. Ribeiro, M. R.; Deffieux, A.; Portela, M. F. Ind Eng Chem Res 1997, 36, 1224.
9. Chien, J. C. W. Topics Catal 1999, 7, 23.
10. Lin, C.-H. Catal Lett 2000, 68, 63.
11. Harrison, D.; Coulter, I. M.; Wang, S.; Nistala, S.; Kuntz, B. A.; Pigeon, M.; Tian, J.; Collins, S. J Mol Catal A Chem 1998, 128, 65.
12. Nishida, H.; Uozumi, T.; Arai, T.; Soga, K. Macromol Rapid Commun 1995, 16, 821.
13. Hong, S. C.; Ban, H. T.; Kishi, N.; Jin, J.; Uozumi, T.; Soga, K. Macromol Chem Phys 1998, 199, 1393.
14. Hong, S. C.; Teranishi, T.; Soga, K. Polymer 1998, 39, 7153.
15. Roscoe, S. B.; Fréchet, J. M. J.; Walzer, J. F.; Dias, A. J. Science 1998, 280, 270.
16. Stork, M.; Koch, M.; Klapper, M.; Müllen, K.; Gregorius, H.; Rief, U. Macromol Rapid Commun 1999, 20, 210.
17. Yu, G. Q.; Zhang, D. Z.; Shun, F.; Qiao, L. J.; Tang, T.; Huang, B. T. Chin Chem Lett 2001, 12, 257.
18. Li, N.-H.; Mazid, M. A. U.S. Pat. 5,168,104, 1992.
19. Hoang, P. P. M.; Russell, C.; Kearns, J. R.; Wanke, S. E.; Lynch, D. T.; Li, N. U.S. Pat. 6,583,082 B2, June 24, 2003.
20. Fuhrmann, H.; Pohl, M.-M. Acta Polym 1993, 44, 156.
21. Sun, L.; Hsu, C. C.; Bacon, D. W. J Polym Sci Part A: Polym Chem 1994, 32, 2135.
22. Jericó, S. J.; Schuchardt, U.; Joekes, I.; Kaminsky, W.; Noll, A. J Mol Catal A Chem 1995, 99, 167.
23. Lynch, D. T.; Wanke, S. E. Can J Chem Eng 1991, 69, 332.
24. Kosek, J.; Grof, Z.; Novák, A.; Štěpánek, F.; Marek, M. Chem Eng Sci 2001, 56, 3951.
25. Chien, J. C. W.; Nozaki, T. J Polym Sci Part A: Polym Chem 1993, 32, 227.
26. Wester, T. S.; Ystenes, M. Macromol Chem Phys 1997, 198, 1623.
27. Galland, G. B.; Seferin, M.; Mauler, R. S.; Dos Santos, J. H. Z. Polym Int 1999, 48, 660.
28. Roos, P.; Meier, G. B.; Samson, J. J.; Weickert, G.; Westerterp, K. R. Macromol Rapid Commun 1997, 18, 319.
29. Kittilsen, P.; McKenna, T. F.; Svendsen, H.; Jakobson, H. A.; Fredriksen, S. W. Chem Eng Sci 2001, 56, 4015.
30. McKenna, T. F.; Soares, J. B. P. Chem Eng Sci 2001, 56, 3931.
31. Galli, P.; Haylock, J. C. Makromol Chem Macromol Symp 1992, 63, 19.
32. Mulder, M. H. M.S. Thesis, University of Alberta, Canada, 1999.